International Journal of Solids and Structures 80 (2016) 297–309

Contents lists available at ScienceDirect

International Journal of Solids and Structures

journal homepage: www.elsevier.com/locate/ijsolstr

Optimization of modular tensegrity structures for high stiffness and frequency separation requirements

Nasseradeen Ashwear*, Ganesh Tamadapu, Anders Eriksson

KTH Mechanics, Royal Institute of Technology, Osquars backe 18, Stockholm SE-100 44, Sweden

ARTICLE INFO

Article history:
Received 4 July 2015
Revised 9 September 2015
Available online 27 November 2015

Keywords:
Tensegrity
Self-stress
Frequency separation
Optimization
Vibration health monitoring

ABSTRACT

Tensegrities are cable-strut assemblies which find their stiffness and self-equilibrium states from the integrity between tension and compression. Low stiffness and coinciding natural frequencies are known issues. Their stiffness can be regulated and improved by changing the level of pre-stress. In vibration health monitoring, the first natural frequency is used as an indicator of better stiffness, but coinciding natural frequencies will be an obstacle in measuring and analysing the correct resonance. In this paper, the above two issues have been considered for modular tensegrity structures. The finite element model used considers not only the axial vibration of the components, but also the transversal vibration where non-linear Euler–Bernoulli beam elements are used for simulations. A genetic algorithm is used to solve the optimization problem, with a multi-objective criterion combination. The optimum self-stress of the tensegrity structures can be chosen such that their lowest natural frequency is high, and separated from others. Two approaches are used to find the optimal self-stress vector: scaling from a base module or considering all modules at once. Both approaches give the same optimum solutions.

1. Introduction

Tensegrities are cable-strut assemblies, which find their stiffness and self-equilibrium states from the integrity between tension in cables and compression in bars. The pre-decided tension in cables and compression in bars are known as unilateral properties of the components. They are classified as class one, where bars do not touch, and class n, where at most n of the bars connect at joints (Motro, 2003; Pinaud et al., 2004).

In the design of these assemblies, normally a Form-Finding process is adapted to which an important contribution was made by Tibert and Pellegrino (2002). Form-Finding is commonly defined as the process of finding an equilibrium and a stable geometry (Faroughi and Tur, 2015). Form-Finding, however, can be seen from different viewpoints, where some methods require the topology and coordinates of the nodes. This is the case when using non-linear programming and force density methods, while other methods use other information sets. For instance, Koohestani (2013) proposed an unconstrained optimization approach for Form-Finding which requires only the connectivity data and a random set of force densities, to form a wide variety of tensegrities with different geometrical and mechanical characteristics.

Although differently defined in literature, Form-Finding is here seen to include the construction of an equilibrium matrix from a given topology and nodal coordinates. Then, the singular value decomposition (SVD) of the equilibrium matrix gives the number of mechanisms m (if any exist) and the dimension of the space of independent self-stress states s. If this self-stress dimension is one, then both the equilibrium and unilateral properties of cables and bars will be easily satisfied by scaling of this single self-stress vector $\boldsymbol{s}$, for a correct design (Schek, 1974; Tran and Lee, 2010a; 2010b). On the other hand, if the dimension of the independent self-stress space is greater than one, feasible self-stress vectors $\boldsymbol{g}$ can be calculated by linear combinations of the calculated self-stress vectors $\boldsymbol{s}_i$ (Schek, 1974; Tran and Lee, 2010b). These must be checked for unilateral conditions, but within these restrictions any linear combination of the $\boldsymbol{s}_i$ vectors is a valid self-stress state. From construction, the basis vectors $\boldsymbol{s}_i$ must be seen as random mutually orthogonal basis vectors for the self-stress state, the linear combinations of which satisfy an internal equilibrium state without external forces.

Tensegrities normally consist of several modules, or stages (Murakami and Nishimura, 2001; Nishimura and Murakami, 2001). These modules, when attached to each other, compose the final tensegrity structure. In the Form-Finding process of multi-module tensegrity structures, there are normally two options:

(i) The first one is to consider the equilibrium matrix of one module and find its feasible self-stress vectors. Then, the complete self-stress vector of the whole structure can be evaluated,

* Corresponding author. Tel.: +46 87906184.
E-mail address: ashwear@mech.kth.se, naser354@hotmail.com (N. Ashwear).

http://dx.doi.org/10.1016/j.ijsolstr.2015.11.017
0020-7683/

taking into account the sharing components between modules, e.g., adding/superposing the values of the elements in the self-stress vector that are corresponding to these sharing elements (Dalilsafaei and Tibert, 2012; Schlaich, 2004) or by scaling the self-stress vector of the basic module and applying it to the other modules. The scaling factors can be chosen based on criteria which lead to an optimum design, or be based on the application requirements (Dalilsafaei et al., 2014; Dalilsafaei and Tibert, 2012). Each module then has a low dimension of its self-stress space, which simplifies this evaluation. On the other hand, the superposition of the results from the module results will demand careful consideration of the support conditions for the modules.

(ii) The second one is to consider the equilibrium matrix of the whole structure (all modules) at once, and to find the self-stress vector by the method described above. For analytical purposes, this option has been commonly adapted as a basic of Form-Finding of tensegrity structures in most of the literature about this subject (Koohestani, 2012; Koohestani and Guest, 2013; Murakami and Nishimura, 2001; Nishimura and Murakami, 2001; Tran and Lee, 2011). This option obviously simplifies the consideration of the support conditions, which can be immediately recognized from the real-life situation, but typically leads to high-dimensional self-stress spaces represented by some excessive $\boldsymbol{s}$ which physically can be interpreted as, some components can be independently pre-stressed. There are some other consideration which can be adapted to enhance this basic approach such as grouping, where grouping can be automated or manual. Recently, Koohestani (2015) developed an automated method for element's grouping and self-stress identification. However, in this study we have used this approach without any predefined grouping of elements. In addition finding a feasible grouping could be an important parameter in the design and optimization of tensegrity structures (Koohestani, 2015).

Both approaches mentioned above for finding the optimum self-stress vector of multi-module tensegrity structure were considered, i.e., we have investigated the impact of following each of the approaches on the optimum design for maximum lowest natural frequency and mode separation requirements. Dalilsafaei et al. (2014) investigated the first approach using bar elements for the modelling, where only axial vibration can be represented. They maximized the lowest natural frequency, without treatment of the coinciding natural frequency problem. Masic and Skelton (2006) demonstrated a method for self-stress optimization.

In literature, researchers focused on minimizing the mass of the structure with consideration of the static situation of the structure. Nagase and Skelton (2014a) provided a unified framework for minimal mass design of tensegrity structures where the design variables were the force densities and the cross-section areas of the components. Good analytical formulas can be found in Skelton and de Oliveira (2009) about the mass minimization of tensegrity structures, where algorithms are given to design an optimal (minimum mass) self-similar structure using self-similar iterations rules.

An important design parameter, which comes into the picture when designing any tensegrity structure is the level of pre-stress. The level of pre-stress can be defined and introduced to tensegrity structures in different ways. But, in general it means an increase or a decrease of the internal forces in the externally unloaded structure. The level of pre-stress represented by ψ, is normally seen as a scalar used to synchronously increase or decrease the internal forces in all components by scaling the self-stress vector $\boldsymbol{g}$, normally expressed as a unit vector. More details about how the pre-stress level can be altered can be found in Ashwear and Eriksson (2014).

The question arises when discussing the optimal self-stress vector, at what level of pre-stress ψ the optimum self-stress vector was found? To generalize the solution, there are two options for setting up the level of pre-stress in the optimization programme: The first one is to normalize the self-stress vector $\boldsymbol{g}$ during the optimization and introduce the level of self-stress ψ as an extra design variable in the optimization, so that the programme will converge to a $\hat{\boldsymbol{g}}$ which is a unit vector scaled by the level of pre-stress ψ. The second option is to consider the constructed $\boldsymbol{g}$ without normalization, in which case the self-stress vector itself contains the level of pre-stress ψ given by the norm of the converged vector $\boldsymbol{g}_\psi = \psi\hat{\boldsymbol{g}}$. In this study we followed the second option and below we will use $\boldsymbol{g}_\psi$ to represent the self-stress vector, including magnitude and distribution between components.

The performed simulations were based on the following assumptions concerning the design. A final topology and geometry was defined, and was connected to a specified pre-stress reference vector, chosen such that the pre-stress forces in the components are found from the scaled vector $\boldsymbol{g}_\psi$. This is considered as implemented by components which are lengthened or shortened from an unstrained length L, introducing axial forces when reaching their design lengths L_s consistent with the externally unloaded geometry of the structure. The nominal design thereby includes a specified exact pre-stress force distribution for a specified exact geometry.

Tensegrity structures are geometrically non-linear structures (Kebiche et al., 1999). Their stiffness can be somewhat regulated and improved by changing the level of pre-stress. In simulations, it is easy to synchronously monitor the lowest natural frequency as an indicator of a high stiffness design, while regulating the level of pre-stress (Ashwear and Eriksson, 2014).

In practice, there are some difficulties. One of these difficulties is that the resonance spectrum of a tensegrity structure normally includes sets of coinciding or very closely situated frequencies, which are resulting from a high degree of symmetry, or repetitivity in the structure. This is particularly true in cases of added modules. In the vibrational health monitoring (VHM) context, where normally only the first natural frequency of the structure is utilized (Guechaichia and Trendafilova, 2011), coinciding natural frequencies will be an obstacle in measuring and analysing the correct resonance. For the VHM purposes, it would be advantageous if the lowest natural frequency of the structure could be easily measured and filtered from the whole spectrum. This aspect has been considered in this paper, where a multi-objective criterion is considered for usage in the optimization programme.

The sensitivity of the first natural frequency to the level of pre-stress in tensegrity structures can be very low depending on the design. For a certain range of pre-stress, the sensitivity of the first natural frequency can sometimes completely vanish (Ali et al., 2010), i.e., this frequency is independent of pre-stress level. The opposite is also true for other tensegrity structures where the higher natural frequencies have a very low sensitivity to the level of pre-stress, while the first natural frequency is very sensitive (Moussa et al., 2001). For this reason, it is not always possible to use the first natural frequency ω_1 in VHM as an indicator of the pre-stress level. We will distinguish the frequencies which are dependent on pre-stress as the sensitive ones.

Unlike the structural optimization problems found in literature which can be classified into, size, shape and topology optimization (Barbosa et al., 2015), with the optimization problem considered in this study, the structure shape, size, and topology will not be one of the optimization variables. The aim of this study was to find the optimum internal force distribution, represented by the scaled self-stress vector $\boldsymbol{g}_\psi$, such that the lowest sensitive natural frequency ω_k of the structure is as high as possible but still well separated from the next higher one ω_{k+1}. The two approaches above were considered and compared. In other words, we discussed how the optimal self-stress vector $\boldsymbol{g}_\psi$ (in the Form-Finding process) of tensegrity structures can be chosen such that their lowest sensitive natural frequency is on one hand relatively high, but on the other hand also well separated from the others. The first objective will ensure that the designed structure

has a relatively high stiffness (Dalilsafaei et al., 2014), while the second objective serves for the VHM purposes (Peeters and De Roeck, 2001). With similar ideas, separation of the natural frequencies is also needed when the objective is to increase the accuracy of the classical damping approximation process (Sultan, 2009).

2. Method of study

In this section, methods for Form-Finding, finite element formulation and optimization setup will be discussed.

2.1. Form and force finding

We here used the Force Density Method (FDM) (Schek, 1974; Tran and Lee, 2010b) (valid for 2-D and 3-D) to find a set of independent self-stress vectors $\boldsymbol{s}_i$, the number dependent on the equilibrium matrix. In this method, the equilibrium matrix $\boldsymbol{A}$ constructed from a known topology and coordinates of one or all the modules (depending on which approach will be followed to find the self-stress vector state $\boldsymbol{g}_\psi$). A singular value decomposition (SVD) of $\boldsymbol{A}$ gives the number of mechanisms m and the independent self-stress states s. The built-in Matlab[1] (version 2013a) function SVD is used, but it is noted that the output from SVD can vary with algorithm, giving different basis vectors of the space.

Support conditions were applied such that they did not create any redundancy in the structure, i.e., if the self-standing structure (with a single module or several modules) has s linearly independent, orthonormalized self-stress vectors, we constrain the structure such that the number s remains.

In the mentioned examples below, two tensegrity structures have been considered and are here used to demonstrate the basic setting. The first is a 2-D four-module X-frame tensegrity, Fig. 1(b), the second a 3-D four-module (four prisms) T-3 tensegrity, Fig. 2(b). The base modules of both structures were designed and supported to have a single state of self-stress ($s = 1$) and one infinitesimal mechanism ($m = 1$). Hence, when constructing a structure of more than one module, any additional module will add one self-stress state to the structure, i.e., in our case $s = 4$ for both cases. The overall self-stress vector $\boldsymbol{g}_\psi$ will be evaluated from $\boldsymbol{s}_0$ of one-module or $\boldsymbol{s}_i$ of the whole structure, by following one of the approaches explained below.

2.1.1. Scaling the base module

In this approach, the equilibrium matrix $\boldsymbol{A}$ is constructed from a known topology and coordinates of the single 'base module'. Then, the SVD of $\boldsymbol{A}$ (with support conditions applied such that $s = 1$ and $m = 1$) gives the unique self-stress unit vector $\boldsymbol{s}_0$ for the base module. Thus, both the equilibrium and the unilateral properties of the components will be easily satisfied by this single self-stress vector $\boldsymbol{s}_0$, for a correct module design.

The self-stress vector $\boldsymbol{s}_i$ of each individual module is then seen as a scaling of the self-stress vector of the base module $\boldsymbol{s}_0$ according to:

$$\boldsymbol{s}_i = a_i \boldsymbol{s}_0 \tag{1}$$

where a_i are the scaling factors for modules, $i = 1, 2, \ldots$. The number of scaling factors equals the number of modules n, i.e., if the tensegrity structure is composed from four modules, there will be four scaling factors, which will be the design variables in the optimization below.

If several or all scaling factors are equal, as implicitly used in literature (grouping), (Tran and Lee, 2010b, 2010c, and many others), then symmetrically located members in the structure will have the same internal force magnitudes. In practice, the scaling factors can be different, according to the application or design requirements.

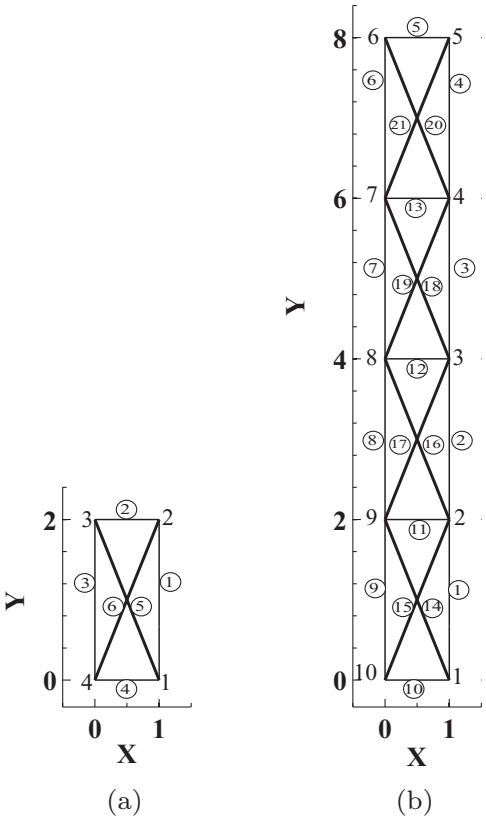

Fig. 1. Topology, coordinates and the numbering scheme of (a) The X-frame base module, (b) Four-module X-frame tensegrity structure.

With this approach, the scaled self-stress vector $\boldsymbol{g}_\psi$ of the whole structure can be written as function of scaling factors a_i and the self-stress vector of the base module $\boldsymbol{s}_0$:

$$\boldsymbol{g}_\psi = \boldsymbol{g}_\psi(a_i, \boldsymbol{s}_0). \tag{2}$$

It is worth noting that in Eq. (2), the pre-stress values of the shared elements (force density $(g_\psi)_i$) between modules are being added together. For example, in the 2-D numerical example given in this study, the value of $(g_\psi)_{11}$ corresponding to the component number 11 in Fig. 1(b) is found by adding s_1^2 to s_2^4, where s_i^m here means the element m in $\boldsymbol{s}_i$ of the module i, as explained in Appendix A. With this setup, the free optimization parameters are the scaling factors a_i. From construction, these are demanded to be non-negative.

2.1.2. All modules at once

In this approach, the equilibrium matrix $\boldsymbol{A}$ valid for the whole structure is constructed from a known topology and the coordinates of all the modules. Then the SVD of $\boldsymbol{A}$ gives a set of s independent self-stress vectors $\boldsymbol{s}_i$ and the number of mechanisms m. For the 2-D and the 3-D examples considered in this study, there were four independent self-stress vector states, $s = 4$. Hence, the feasible self-stress vectors $\boldsymbol{g}_\psi$ can be calculated by any linear combination of the basis vectors $\boldsymbol{s}_i$.

$$\boldsymbol{g}_\psi = \sum_{i=1}^{s} b_i \boldsymbol{s}_i \tag{3}$$

[1] The MathWorks, Inc., Natick, U.S.A.

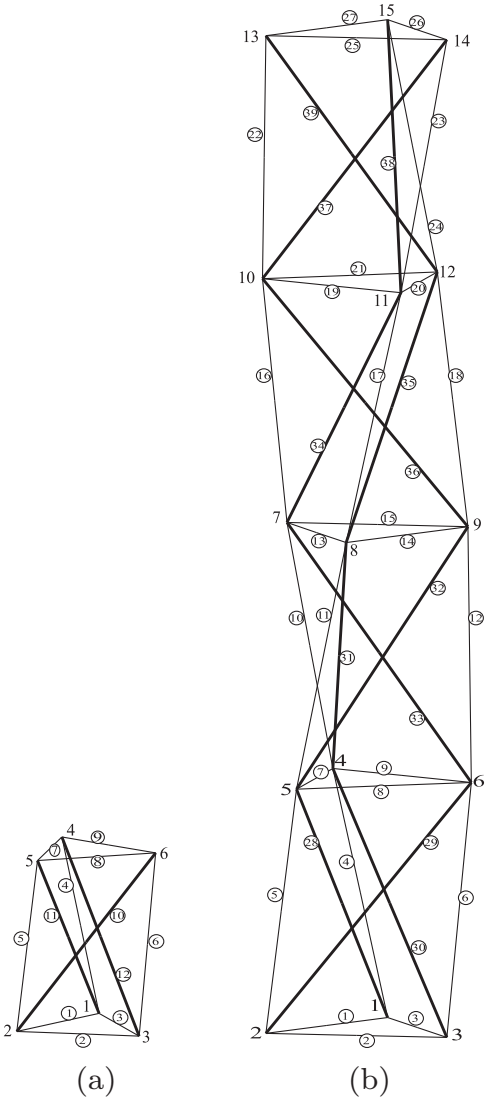

Fig. 2. Topology and the numbering scheme of (a) The base module of T-3 tensegrity, (b) Four-module T-3 tensegrity structure.

where b_i are the coefficients of independent self-stress modes $\boldsymbol{s}_i$. As the basis vectors must be seen as random outputs from the SVD algorithm used, these coefficients can well be negative, as long as unilateral constraints are fulfilled for the whole. With $\boldsymbol{s}_i$ combined, and the unilateral and stability conditions being satisfied, the free optimization parameters are the coefficients b_i.

It is noted that the number of design variables is equal in the two approaches, but refer to different basic self-stress vectors. One also notes that the $\boldsymbol{s}_o$ contributions in the first approach, suitably combined, gives one way to define the basis of the space. It is worth to mention that only this approach is possible to use in the case of a general tensegrity (non modular) with several states of self-stress.

In the present work, the aim is to find $\boldsymbol{g}_\psi$, Eq. (2) or (3) by finding the scaling factors a_i in Eq. (2), or the linear combination coefficients b_i in Eq. (3), such that the lowest sensitive natural frequency ω_k is high and well separated from the next higher natural frequency ω_{k+1}. This was achieved by applying a Genetic Algorithm (GA) (Holland, 1975), from the built-in functions of Matlab, as explained in the optimization section below.

2.2. Finite element formulation

Having found a scaled self-stress vector $\boldsymbol{g}_\psi$ by means of either of Eq. (2) or (3), the unstrained length of a jth component L_j can be found. Each element $(g_\psi)_j$ in the self-stress vector $\boldsymbol{g}_\psi$ represents the force density corresponding to component j in the structure, $(g_\psi)_j = N_j/L_j^s$, (Vassart and Motro, 1999), where N_j is the axial internal force and L_j^s is the designed length of the component j, which is known in advance. But $N_j = EA_j(L_j^s - L_j)/L_j$ from which the unstrained length L_j can be calculated as:

$$L_j = EA_jL_j^s/(N_j + EA_j) \tag{4}$$

where, $N_j = (g_\psi)_jL_j^s$. This can be seen as a definition of an initial strain of the defined geometry.

When each component of the structure is divided into several computational finite elements (Ashwear and Eriksson, 2014; Eriksson, 1997), the unstrained length for each finite element l can be found from $l = L_j/n$, where n is the number of elements per component. In the present implementation, $n = 4$ for compressed members, and $n = 2$ for tensioned members.

The members of tensegrity structures are commonly in literature seen as pin-jointed bar elements, where no bending moments affect components. With this formulation, only the axial response can be captured. In a health monitoring context, where essentially the resonance spectrum is triggered by external excitation, the most visible modes will, however, be the transversal modes of vibration. In simulations, this consideration must see the components as having a bending behaviour, and a member stiffness affected by the current axial force.

We have used a non-linear Euler–Bernoulli beam element for modelling both compressed (bar) and tensioned (cable) elements with assumed physical data for sectional properties. In a tensioned component the (low) bending stiffness will to a very low degree affect the response.

The geometric non-linearity has been considered in the internal forces. This gives consequences for the tangent element stiffness matrix $\boldsymbol{k}_T$, which has been decomposed into an element elastic stiffness matrix $\boldsymbol{k}_E$ and a geometric stiffness matrix $\boldsymbol{k}_G$, according to:

$$\boldsymbol{k}_T = \boldsymbol{k}_E + \boldsymbol{k}_G \tag{5}$$

It is well known that a string is tuned to its right resonance by introduction of an axial force. Similarly, the resonance is affected by a compressive force, and the resonance frequency lowered with increasing force magnitude. The element geometric stiffness matrix $\boldsymbol{k}_G$ was formulated to include the effect of the axial force on the transversal stiffness of the beam element. The one-way coupling between the axial force and the transversal stiffness emphasized the non-linearity of the tensegrity structure response.

The structural tangent stiffness matrix $\boldsymbol{K}_T$ is conventionally assembled according to the symbolic expression:

$$\boldsymbol{K}_T = \sum \boldsymbol{L}\boldsymbol{T}\boldsymbol{k}_T\boldsymbol{T}^T\boldsymbol{L}^T \tag{6}$$

where $\boldsymbol{L}$ is the element connectivity matrix, defined from topology, and $\boldsymbol{k}_T$ the element tangent stiffness matrix Eq. (5), while $\boldsymbol{T}$ is the transformation matrix from local to global degrees of freedom, formulated for 2-D and 3-D as in Kattan (2007, Chaps. 8 and 10), respectively. The sum extends over all elements.

For the 2-D case, using N_o as the elastic normal force, A the cross-sectional area, l the element unstrained length and I the relevant

moment of inertia, the formulation of $\boldsymbol{k}_E$ and $\boldsymbol{k}_G$ is well-known and can be found in Paultre (2010, Chap. 14), and their mathematical expressions can be found in Ashwear and Eriksson (2014).

The linear 2-D beam element mass matrix $\boldsymbol{m}$ was formulated according to well-known expressions, (Argyris and Mlejnek, 1991, chap. 3), and its mathematical expression can be found in Ashwear and Eriksson (2014) using ρ as the material density. This consistent mass matrix is used for all elements. The structural mass matrix $\boldsymbol{M}$ is similarly assembled according to the symbolic expression:

$$\boldsymbol{M} = \sum \boldsymbol{L}\boldsymbol{T}\boldsymbol{m}\boldsymbol{T}^T\boldsymbol{L}^T \tag{7}$$

For the 3-D case, the same formulation steps can be followed to find the tangent stiffness and mass matrices. The 3-D elastic, geometric and mass matrices are given in Appendix B.

Having $\boldsymbol{K}_T$ and $\boldsymbol{M}$ assembled at a non-linear equilibrium state (more details about equilibrium iterations can be found in Ashwear and Eriksson (2014)) for a chosen internal pre-stress $\boldsymbol{g}_\psi$, but no external forces, the vibration problem of the structure can be linearized. The small free undamped vibrations of the structure around the evaluated equilibrium state are thereby obtained from the generalized eigenproblem:

$$-\omega_k^2\boldsymbol{M}\boldsymbol{\phi}_k + \boldsymbol{K}_T\boldsymbol{\phi}_k = 0 \tag{8}$$

where ω_k^2 is one of the n eigenvalues and $\boldsymbol{\phi}_k$ the corresponding eigenvector, with n the number of active degrees of freedom. The eigenvalues were ordered so that $\omega_1 \le \omega_2 \cdots \le \omega_n$. The spectral decomposition thereby gives n natural frequencies ω_k and the related eigenvectors $\boldsymbol{\phi}_k$ of the structure at the considered equilibrium state. As the tensegrity structures normally contain a high degree of symmetry, the resonance solutions will normally contain sets of closely situated frequencies, and possibly eigenspaces of higher dimensions (Strang, 1988).

2.3. Optimization problem

The optimal scaling factors a_i in Eq. (2) and the linear combination coefficients b_i in Eq. (3), have been found using a genetic algorithm included in the Matlab software. Being in formulation a two-objective optimization, where a Pareto front is the complete result, (Caramia and Dell'Olmo, 2008), a weighted sum method for making the multi-objective optimization into a single objective one has been used as:

$$\begin{aligned} &\text{minimize} \quad \frac{\alpha}{\omega_k(\boldsymbol{g}_\psi)} + \frac{\beta}{\omega_{k+1}(\boldsymbol{g}_\psi) - \omega_k(\boldsymbol{g}_\psi)} \\ &\boldsymbol{g}_\psi = \boldsymbol{g}_\psi(a_i, \boldsymbol{s}_0) \;\text{ or }\; \boldsymbol{g}_\psi = \sum_{i=1}^{s} b_i \boldsymbol{s}_i \\ &\qquad \text{subject to} \quad (g_\psi)_j > 0 \qquad \forall j \in \text{Cables} \\ &\qquad\qquad\qquad\quad (g_\psi)_j < 0 \qquad \forall j \in \text{Bars} \\ &\qquad\qquad\qquad\quad a_i > 0 \qquad \text{(if Eq. (1) is used)} \end{aligned} \tag{9}$$

where α and β are the objective function weights. More details about multi-objective optimization can be found in Barbosa et al. (2015).

While using the first approach the only constraint applied is that the variables a_i are positive, as the unilateral constraints are immediately fulfilled. In the second approach, the constraints in the GA were handled as follows. Let

$$\boldsymbol{s}_i = \begin{bmatrix} \boldsymbol{s}_i^c \\ \boldsymbol{s}_i^b \end{bmatrix}$$

where $\boldsymbol{s}_i^c$ and $\boldsymbol{s}_i^b$ are the component parts of the self-stress vector $\boldsymbol{s}_i$ corresponding to the cables and bars, respectively. Then, the input linear inequality constraints to GA can be given in the form $\boldsymbol{A}\boldsymbol{X} \le \boldsymbol{0}$, where

$$\boldsymbol{A} = \begin{bmatrix} -\boldsymbol{s}_1^c & -\boldsymbol{s}_2^c & \cdots & -\boldsymbol{s}_s^c \\ \boldsymbol{s}_1^b & \boldsymbol{s}_2^b & \cdots & \boldsymbol{s}_s^b \end{bmatrix} \quad \text{and} \quad \boldsymbol{X} = [b_1, b_2, \cdots, b_s]^{\mathrm{T}}.$$

The tangent stiffness matrix singularity was handled by assigning a large fitness value (estimated from multiple runs).

The eigenvalue ω_k is the lowest natural frequency that is sensitive to the change in the level of pre-stress ψ defined as before (normally it is the first natural frequency ω_1, but for some cases it is the higher natural frequency ω_2 when the lowest frequency is independent of pre-stress). Following usual practice to choose weights summing to one, in this study we chose $\alpha = 0.2$ and $\beta = 0.8$, but other choices are fully possible. However, depending on the nature of the structure, the values of the objective function weights (α and β) are decided. For instance, in both examples considered in this study, it was more difficult to separate the first sensitive natural frequencies than maximizing the first one, and for this reason β is greater than α. It is noted that the obtained optimal solutions normally will vary continuously with the choice of α and $\beta = 1 - \alpha$, allowing an easy tuning of obtained results, if the balance between the relative weighting of the criteria is re-considered. Such a change of weighting will essentially represent a movement along the Pareto front representing the solution to the two-criterion optimization.

When a self-stress vector $\boldsymbol{g}_\psi$ is computed, the unilateral properties of each component and the stability of the structure are evaluated. With the finite element formulation used, approaching the critical load of buckling is very well detected by at least one of the eigenvalues of the tangent stiffness matrix approaching zero. But we also applied a factor of safety of 20% such that in the final design (the optimal), the internal forces in the bars will always be well below their Euler buckling loads.

The optimal design must fulfil not only the VHM requirements (natural frequencies separation) but also the load carrying capacity of the structure. It is noted that if we run the optimization programme with only the conditions mentioned above and the constraints mentioned in Eq. (9), the programme will converge to a solution where the top module will have very low internal forces, limiting the structure load carrying capacity, and perhaps even more the stiffness, due to low pre-stress in the top module. For this reason, another condition has been added such that the horizontal static displacement in the x direction (δ_x) of the top nodes resulting from the application of specified external load F_x at these nodes, must be less than a certain value δ_x, where in reality the application requirements prescribe the values of F_x and δ_x. In the present work, the value of δ_x has been taken as for the structure with symmetric self-stress design, so that the optimization dose not lead to a less functional structure. For self-stress vectors $\boldsymbol{g}_\psi$ not fulfilling the above requirements, a very large objective function value was assigned so that they have very low chance to pass to the next generations.

It is well known that the performance and efficiency of a genetic algorithm depends on some basic parameters. The parameters used in this study are given in Table 1, related to the specification of the Matlab GA tool, where, e.g., the binary coding of variables is inherent.

Table 1
Basic parameters of the genetic algorithm used in this study.

Parameter name	Type and value
Bounds of variables	To be positive in the first approach, no bounds in the second approach
Population (type, size)	Double vector, see figures for the sizes
Selection (function)	Stochastic uniform
Crossover (type, ratio)	Heuristic, 1.2 (the default value)
Mutation (function)	Adaptive feasible
Stopping criterion	The number of generation

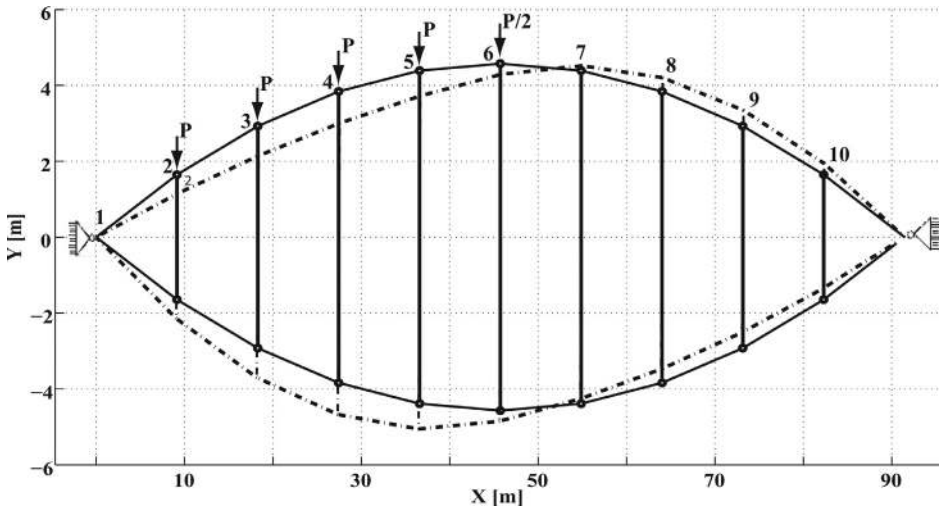

Fig. 3. Deformed and undeformed (dashed line) shape of the cable girder (deflections enlarged for visibility).

While solving the optimization problem given in Eq. (9) using GA, the algorithm provided different results in different runs. For this reason we have run the algorithm in each example several times. But for brevity we only give a typical run for each example, which converged towards what we have good reasons to believe is the global optimum.

3. Finite element verification

The objective of this section is only to verify the 3-D finite element formulation used in this study. The verification of the 2-D formulation can be found in Ashwear and Eriksson (2014).

The 2-D pre-stressed cable girder, Fig. 3, and the 3-D hyperbolic paraboloid, Fig. 5, were analysed by Buchholdt (1969); Lewis et al. (1984) and others, to find the displacements under joints in the direction of applied load *P*. For the verification purpose of the 3-D finite element formulation, we have analysed both structures. We also used the tangent stiffness matrix evaluated at the pre-stressed but externally unloaded equilibrium state, and the mass matrix to solve for the eigenvalues ω_k^2, Eq. (8).

3.1. Pre-stressed cable girder example

A 2-D pre-stressed cable girder, Fig. 3, is symmetric about the vertical and horizontal centre lines.

The girder was here seen as a tensegrity structure. It gains its stability from the integrity between compression force in bars and tension force in cables, and there is no bending moment effect at its physical joints. It is unsymmetrically loaded by the load $P = 44.8$ kN, cf. Fig. 3. The girder has a span and depth of 91.44 m and 9.14 m, respectively. Bars, top cables and bottom cables have a cross sectional area of 1290.3 mm^2, 1045.2 mm^2 and 2090.3 mm^2, respectively. The same material was used for top and bottom cables with Young's modulus $E = 165.55$ GPa, while for bars $E = 209.92$ GPa, with $\rho = 7500$ kg/m^3 and Poisson's ratio $\nu = 0.30$ for all components. More details about the structure can be found in Buchholdt (1969), Lewis et al. (1984). It is worth noting that all the degrees of freedom in the *z* direction were constrained for this 2-D example. The rotational degrees of freedom must be released at joints where several elements meet (Ashwear and Eriksson, 2014, 2015). The tension coefficient applied was 35.016 kN/m.

The joint displacements calculated by the finite element formulation used in this study, the dynamic relaxation method (Lewis et al., 1984) and the steepest descent method (Buchholdt, 1969) are shown in Table 2 and they are in very good agreement. The three lowest natural frequencies and the corresponding mode shapes of the cable girder are shown in Fig. 4. The mode shapes are found to be similar to those for a simply supported beam.

3.2. Hyperbolic paraboloid network

The 3-D hyperbolic paraboloid shown in Fig. 5 was analysed by many researchers to find the deflection under the applied load $P = 0.0157$ kN. Lewis et al. (1984) numerically analysed this structure by using the dynamic relaxation method, and experimentally verified the results. Another solution was found by Kwan (1996). We analysed

Table 2
Comparison of cable girder displacements relative to the unloaded structure's coordinates.

	Displacements of the top cable (m)		
Node no.	Beam elements (present)	Steepest descent (Buchholdt, 1969)	Dynamic relaxation (Lewis et al., 1984)
2	0.4984	0.4946	0.4980
3	0.7777	0.7804	0.7762
4	0.8342	0.8338	0.8362
5	0.6677	0.6700	0.6668
6	0.2795	0.2791	0.2795
7	−0.1293	−0.1270	−0.1294
8	−0.3604	−0.3542	−0.3588
9	−0.4145	−0.4144	−0.4126
10	−0.2938	−0.2926	−0.2920

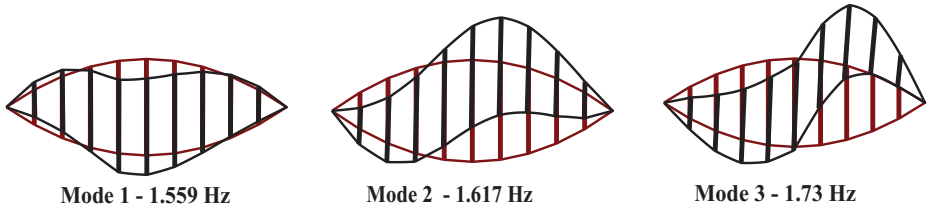

Fig. 4. The first three mode shapes of the cable girder.

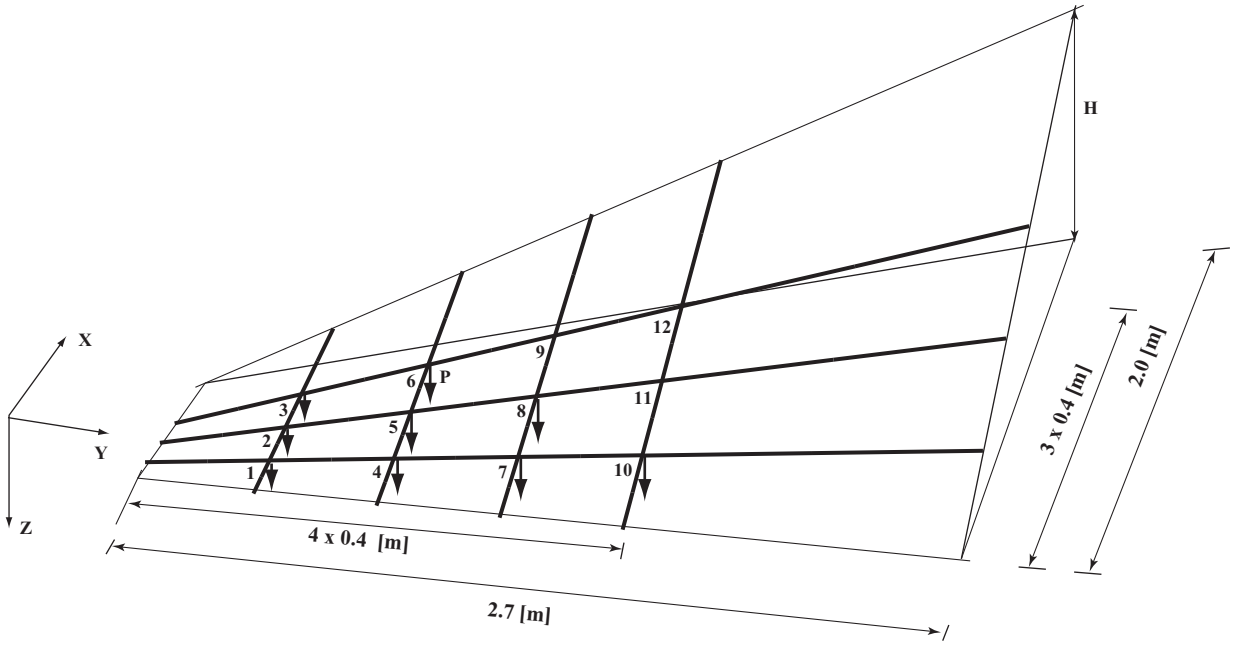

Fig. 5. Hyperbolic paraboloid network.

the hyperbolic paraboloid as another verification example of the 3-D finite element formulation used in the present work.

The hyperbolic paraboloid cables have a cross sectional area of 0.785 mm^2, Young's modulus $E = 128.30\,GPa$ with $\nu = 0.30$, and $\rho = 7500\,kg/m^3$, for all components. The corner rise was chosen as $H = 0.45\,m$ and an average pre-stress of 0.20 kN was applied in all members. Results from the present and other studies are presented in Table 3. Results for the lowest natural frequencies and mode shapes are shown in Fig. 6.

4. Numerical examples

Two tensegrity structures have been considered, a 2-D T13C8 four-module X-frame tensegrity structure, Fig. 1(b), where the notation T_x and C_y gives the numbers of tensile and compressive components in the structure, and a 3-D four-module (four prisms) T-3 tensegrity structure, Fig. 2(b). In each example, the self-stress vector $\boldsymbol{g}_\psi$ in the optimization problem Eq. (9), was calculated using the above two approaches of study.

For both examples, we have presented the optimum solution based on two approaches and compared them with an non-optimum solution. In the optimum frequency spectrum, the lowest pre-stress sensitive natural frequency is well separated from the next level of frequencies and higher than the non-optimal solution.

The equilibrium matrix $\boldsymbol{A}$ for the base module or for the whole structure in both examples below, was calculated by using the method in Tran and Lee (2010b), Schek (1974) with topology and coordinates known in advance.

In the numerical calculations below, the material for all cables and bars was defined by the elastic modulus $E = 210\,GPa$, Poisson's ratio $\nu = 0.30$, and density $\rho = 7850\,kg/m^3$.

By the symmetry of the structures considered for the present analysis, the force density in the bars in each module are equal. In the first approach, the self-stress vector of the base module $\boldsymbol{s}_o$ is normalized with the force density of the bars. For this reason the values of scaling factors a_i and the force density $(g_\psi)_i$ of the bars in each module are equal. In the second approach, the values of the linear coefficients change with self-stress basis $\boldsymbol{s}_i$, which are highly dependent on the computation algorithm for SVD of the equilibrium matrix. Therefore, we have presented non-optimal and optimal solutions from both approaches in the form of the force density in one diagonal bar for each module; from these, the whole pre-stress pattern can be calculated.

4.1. Example 1, a 2-D four-module tensegrity

The plane tensegrity structure shown in Fig. 1(b) is composed of four X-frame modules, with a designed size of $1 \times 2\,m^2$ for each module, Fig. 1(a). When all modules are connected together, they compose the target structure with a designed size of $1 \times 8\,m^2$. Massive circular bars and cables were used with a diameter of 0.05 m and 0.015 m, respectively. It was assumed that the structure was designed to carry an external horizontal load $F_x = 4\,kN$ equally divided on the top nodes 5 and 6. The maximum horizontal static displacement allowed was chosen to be $\delta_x = 0.052$ m. For support conditions, node number 1 is fixed in X and Y directions and node number 10 is fixed in Y direction.

With these design parameters, it was observed that the first natural frequency of this structure is almost independent of the level of pre-stress, and relates to a global bending mode of vibration. This

Table 3
Comparison of hypar displacements relative to the unloaded structure's coordinates.

	Deflection Z (mm)			
Node no.	Beam elements (present)	Another method (Kwan, 1996)	Dynamic relaxation (Lewis et al., 1984)	Experimental (Lewis et al., 1984)
1	19.29	19.52	19.30	19.50
2	25.46	25.35	25.30	25.30
3	23.27	23.31	23.00	22.80
4	25.68	25.86	25.90	25.40
5	33.83	34.05	33.80	33.60
6	29.46	29.49	29.40	28.80
7	25.74	25.79	26.40	25.20
8	31.32	31.31	31.70	30.60
9	21.57	21.42	21.90	21.00
10	21.54	21.48	21.90	21.00
11	20.25	20.00	20.85	19.80
12	14.90	14.40	14.80	14.20

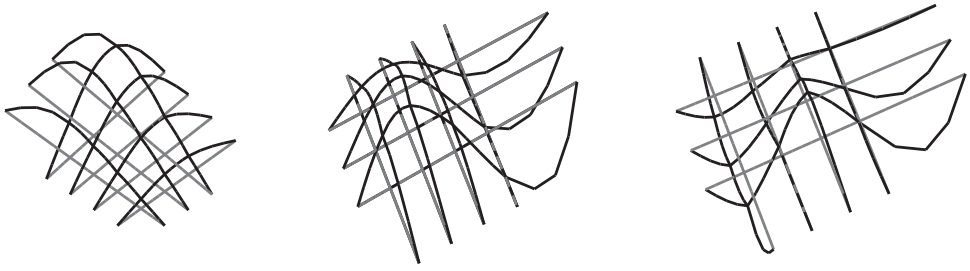

Mode 1 - 44.43 Hz **Mode 2 - 51.32 Hz** **Mode 3 - 90.23 Hz**

Fig. 6. The first three mode shapes of the hypar net.

frequency is well separated from the other higher frequencies. Therefore, we used $\omega_k = \omega_2$ in the optimization problem Eq. (9), i.e., we maximized ω_2 and separated it from ω_3.

Using the first approach, the self-stress vector for the separated base module $\boldsymbol{s}_0$ was calculated from the SVD of the equilibrium matrix $\boldsymbol{A}$ for known topology and coordinates, Fig. 1(a). Then, the self-stress vector $\boldsymbol{g}_\psi$ of the whole structure was found by using Eq. (2).

Symmetrical force density distribution pattern such as $(g_\psi)_i = 50$ kN/m in all the bars (diagonals), gives close to coinciding natural frequencies, $f_2 = 10.318$ Hz and $f_3 = 10.347$ Hz ($f_k = \omega_k/2\pi$).

The force density distribution in the bars for each module from bottom to top obtained using the optimum scaling factors a_i, is $(g_\psi)_i = (4.650, 4.612, 4.252, 4.151)$ kN/m, respectively. The optimum natural frequencies obtained for this force density distribution are $f_2 = 18.558$ Hz and $f_3 = 19.316 textHz$. They are relatively high and well separated compared with the above values for non-optimal design. The results of the first six lowest natural frequencies for both the arbitrary (non-optimal) design and for the optimal design are shown in Fig. 7(a). Fig. 7(b) illustrates the history of fitness function vs the generations for a typical run of this example using scaling from a base module approach.

In the second approach, the equilibrium matrix $\boldsymbol{A}$ of the whole structure was considered with the topology and coordinates shown in Fig. 1(b). The SVD of $\boldsymbol{A}$ gave four independent self-stress vectors $\boldsymbol{s}_i$. Hence, there are four linear combination coefficients b_i. Then, the self-stress vector $\boldsymbol{g}_\psi$ was calculated using Eq. (3). An example of non-optimal design is when the linear combination coefficients chosen such that they give a symmetric self-stress vector. For instance, when the force density in all bars $(g_\psi)_i = 40$ kN/m, the natural frequencies are $f_2 = 12.681$ Hz and $f_3 = 12.733$ Hz, which are very close. However, it is interesting to compare the two non-optimal examples given for this structure. The natural frequency decreased with increase in the prestress (from 40 kN/m to 50 kN/m), because of the bar dominated mode of vibration for this frequency (Ashwear and Eriksson, 2014).

Optimum values of the linear combination coefficients were found to give a force density in the bars $(g_\psi)_i = (4.647, 4.599, 4.201, 4.099)$ kN/m, respectively, gives natural frequencies of $f_2 = 18.592$ Hz and $f_3 = 19.218$ Hz. It is interesting to note that these natural frequencies are very close to the optimum values obtained from the first approach. It is obvious that the approaches would converge to the same optimal solution, and that the small differences in results shown rather give an indication of the accuracy in the GA algorithm. Results from the linear combination approach for both non-optimal and optimal solutions are shown in Fig. 8(a) for the first six lowest natural frequencies. The history of fitness function vs the generations for a typical run of this example is depicted in Fig. 8(b).

4.2. Example 2, a 3-D four-module T-3 tensegrity prism

The T-3 based tensegrity structure shown in Fig. 2(b) was chosen as a 3-D example in this study. It consists of four T-3 prisms, Fig. 2(a). It is made up of 39 components, 12 bars and 27 cables, with 15 nodes whose coordinates are listed in Table 4. All bars and cables were massively circular with diameters of 0.065 m and 0.015 m, respectively. Support conditions applied here are essential to the six rigid body mechanisms. We defined node 1 as completely fixed, node 2 fixed in Y and Z directions and node 3 fixed in Z direction.

The external load F_x applied at each node of the top triangle was assumed to be 700 N. The maximum horizontal static displacement allowed for each of them was chosen to be $\delta_x = 0.032$ m.

In the first approach, the equilibrium matrix $\boldsymbol{A}$ of the base module was calculated following the method in Tran and Lee (2010b),

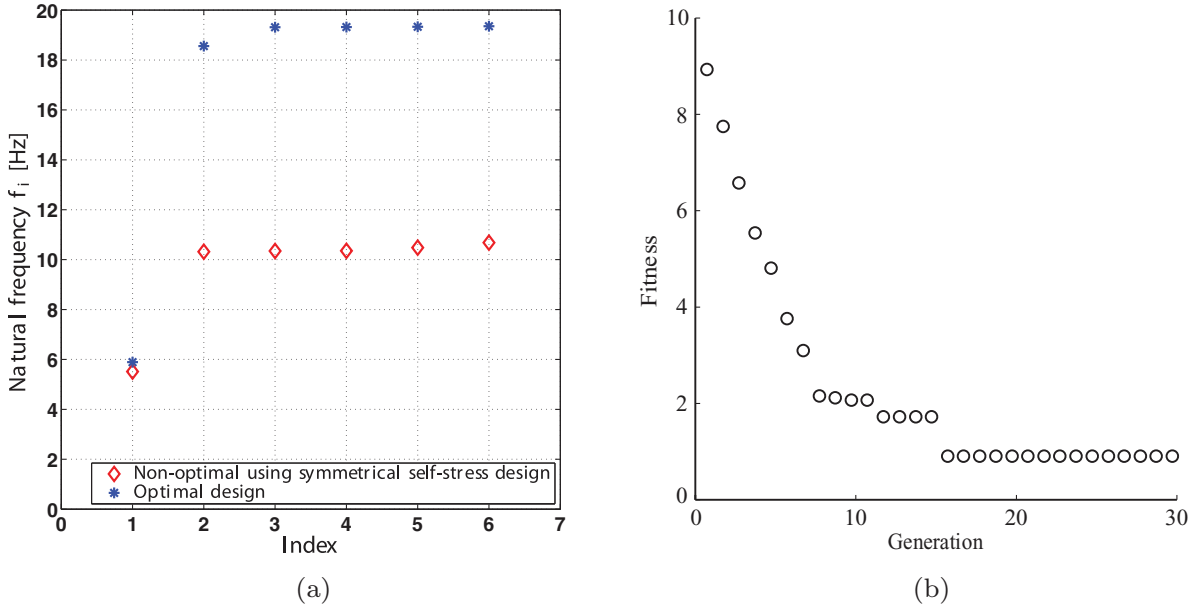

Fig. 7. (a) Natural frequencies distribution for non-optimal and optimal designs of the structure in Fig. 1(b) using the scaling from a base module approach, where the second and third natural frequencies are separated. (b) History of fitness vs generation number for a typical run.

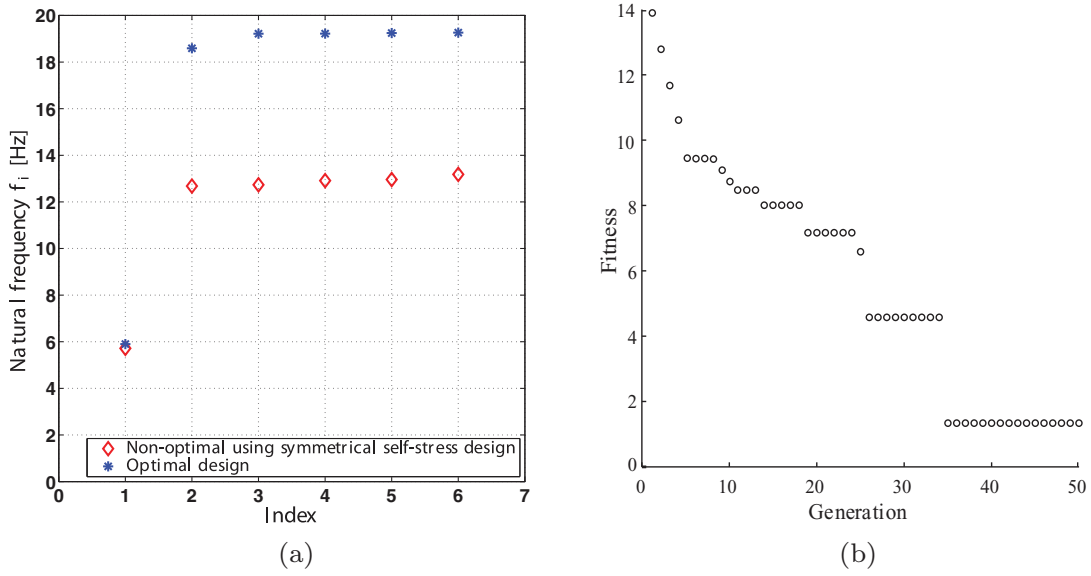

Fig. 8. (a) Natural frequencies distribution for non-optimal and optimal designs of the structure in Fig. 1(b) using the linear combination approach, the second and third natural frequencies are separated. (b) History of fitness vs generation number for a typical run.

Schek (1974), with the topology of the base module as shown in Fig. 2(a) with coordinates for the six nodes in Table 4. Then, the SVD of $\boldsymbol{A}$ gives the self-stress vector $\boldsymbol{s}_0$ which satisfies the unilateral conditions of both the bars and the cables. The self-stress vector $\boldsymbol{g}_\psi$ for the whole structure was calculated following the same strategy explained in the 2-D example above. As this structure consists of four modules, there will be four scaling factors, a_1, a_2, a_3 and a_4.

One example of non-optimal structure with symmetrical self-stress vector (commonly used in literature when a grouping strategy is adapted), e.g., if the forces densities $(g_\psi)_i$ in all bars are equal to 40 kN/m. The symmetric self-stress vector gives almost coinciding natural frequencies $f_1 = 0.734$ Hz and $f_2 = 0.744$ Hz. This situation, however, can be avoided by the proposed method of optimization.

The optimum design, using $\alpha = 0.2$ and $\beta = 0.8$ in Eq. (9), was obtained with the force density in all bars of each module from bottom to top, $(g_\psi)_i = (142.701, 122.130, 94.100, 41.952)$ kN/m, respectively. The corresponding natural frequencies obtained are $f_1 = 2.577$ Hz and $f_2 = 2.957$ Hz, which are higher and more well separated than those for the non-optimal pre-stress. The six lowest natural frequencies for both the symmetrical self-stress vector and for the optimal design are shown in Fig. 9(a). The history of fitness function vs the generations for one typical run of this example using the first approach is showing in Fig. 9(b).

When using the second approach, the equilibrium matrix $\boldsymbol{A}$ of the whole structure was calculated from the topology and coordinates of the whole structure given in Fig. 2(b) and Table 4, respectively. Then, the SVD of $\boldsymbol{A}$ gives four independent self-stress vectors $\boldsymbol{s}_i$. The self-stress vector $\boldsymbol{g}_\psi$ can be any linear combination between $\boldsymbol{s}_i$, Eq. (3). Four linear combination coefficients b_i are sought, such that the resulting $\boldsymbol{g}_\psi$ satisfies the unilateral conditions, the stability of the structure and the static displacement δ_x (defined as before), with higher natural frequencies, and with the first ones being separated.

Table 4
Nodal coordinates of the three-module T-3 tensegrity structure shown in Fig. 2(b).

Coordinates (m)			
Node no.	X	Y	Z
1	0.50	0.00	0.00
2	−0.25	0.433	0.00
3	−0.25	−0.433	0.00
4	0.433	0.25	2.00
5	−0.433	0.25	2.00
6	0.00	−0.50	2.00
7	0.25	0.433	4.00
8	−0.50	0.00	4.00
9	0.25	−0.43	4.00
10	0.00	0.50	6.00
11	−0.433	−0.25	6.00
12	0.433	−0.25	6.00
13	−0.25	0.433	8.00
14	−0.25	−0.433	8.00
15	0.50	0.00	8.00

With the self-stress base vectors obtained from Matlab SVD, choosing linear combination coefficients b_i that give a symmetric self-stress vector, leads to coinciding natural frequencies. For example, if the linear combination coefficients are chosen such that the force density in all bars equal 40 kN/m, which found to give coinciding natural frequencies as in the first approach.

The optimal solution obtained with $\alpha = 0.2$ and $\beta = 0.8$ in Eq. (9), gave the force density in the bars of each module from the bottom to the top of the structure $(g_\psi)_i = (141.150, 121.519, 93.470, 41.626)$ kN/m, respectively. With this design, the natural frequencies are $f_1 = 2.552$ Hz and $f_2 = 2.939$ Hz. These natural frequencies are relatively high and well separated. They are also approximately the same as the optimum natural frequencies obtained from the first approach for this structure. The first six natural frequencies for both the arbitrary (non-optimal) design and for the optimal one are shown in Fig. 10(a). Fig. 10(b) shows the history of fitness function vs the generations for a typical run of this example using the second approach.

5. Discussion

In the design of tensegrity structures, a process known as Form-Finding is adapted. This process has been considered by many authors in literature, but with different strategies and definitions adapted. The Form-Finding is employed to find the internal force distribution for either pre-decided shape (Tran and Lee, 2010b; 2010c, and many others), or to find it such that the internal equilibrium is satisfied but for many different shapes and for a certain topology (Koohestani, 2013). Normally, these methods of Form-Finding lead to structures with resonance spectra including sets of coinciding or very closely situated frequencies, where the symmetric pre-stress vector yielded from the Form-Finding process is one of the causes. This is particularly the case for tensegrity structures built from modular units.

The Form-Finding in this study was performed for a known topology and coordinates (final shape). Each approach used in this present work to find the optimum self-stress vector $\boldsymbol{g}_\psi$, can provide an infinite number of solutions, which all satisfy the unilateral conditions of cables and bars, but these need to be checked also for the structure equilibrium requirement. The new aspect in this study is that, in addition to satisfying the unilateral properties of the components and the stability of the structure, in the Form-Finding we choose the internal equilibrium such that the low frequencies of the structure are separated and the lowest one is being maximised for a certain combination of a level of pre-stress ψ and a self-stress vector $\boldsymbol{g}$ represented in this study by the scaled vector $\boldsymbol{g}_\psi$.

We have used two approaches to describe the self-stress vector $\boldsymbol{g}_\psi$ with different basis vectors, but with equal numbers of design variables. A genetic algorithm was used to find the optimum vector through finding a_i in the first approach and b_i in the second approach. Results from both approaches were found to be approximately equal in terms of natural frequencies values and separation. The minor differences should be seen as a lack of final convergence of GA algorithm. This observation increases the confidence in the optimum solutions we have got.

It is noted that, the convergence of GA when using the first approach (scaling from a base module), is faster than when using the second approach (linear combination), which attributed to the fact that the variable space in the first approach is bounded to be positive.

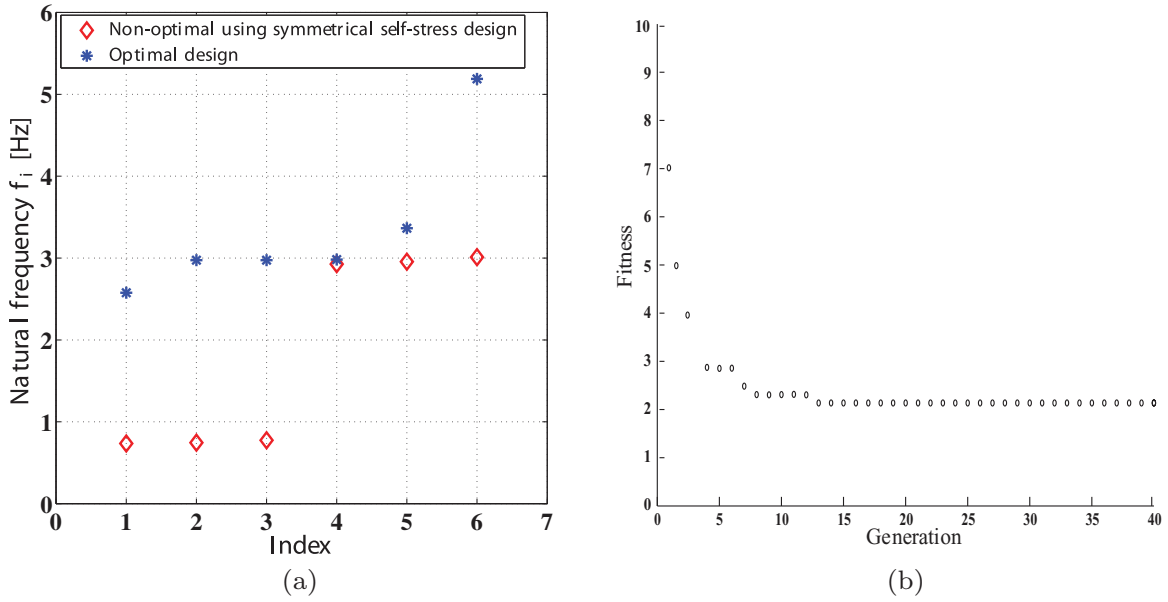

Fig. 9. (a) Natural frequencies distribution for non-optimal and optimal designs of the structure in Fig. 2(b) using the scaling from a base module approach, the first and second natural frequencies are separated. (b) History of fitness vs generation number for a typical run.

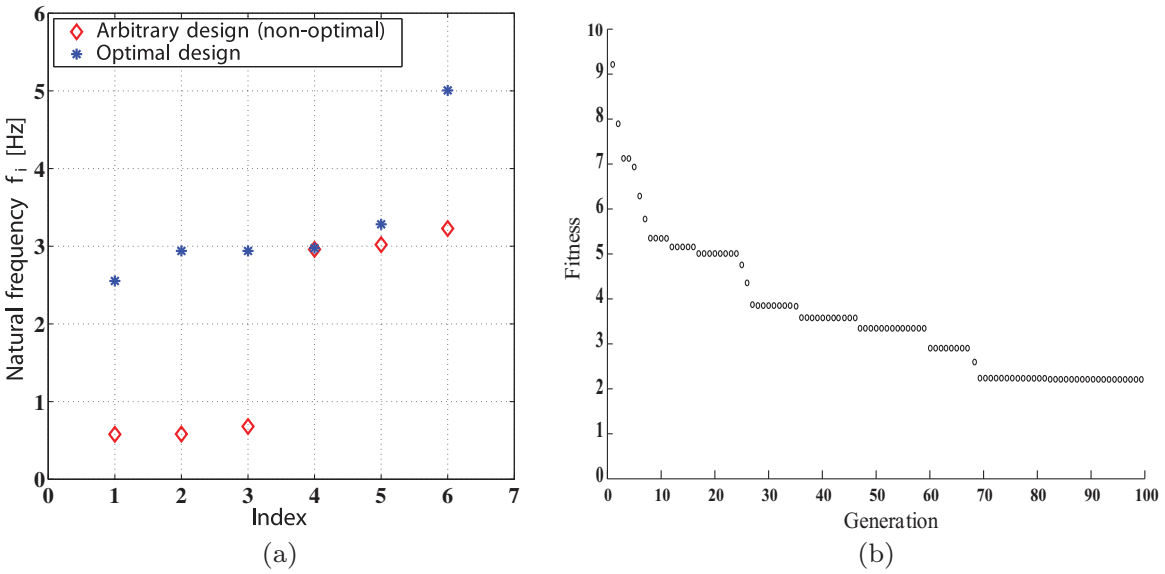

Fig. 10. (a) Natural frequencies distribution for non-optimal and optimal designs of the structure in Fig. 2(b) using the linear combination approach, where the first and the second natural frequencies are separated. (b) History of fitness vs generation number for a typical run.

6. Conclusion and future work

Low stiffness and coinciding frequencies are known characteristics of tensegrity structures, in particular when a symmetric self-stress design is adapted. It has been proved that these two issues can be avoided in the early stage of design (in the form-finding stage).

The nature of the optimization problem is non-convex, implying that there is no guarantee that the results given here represent global optimal solutions. But we relied on repeated solutions and similarity of the results from the two approaches to increase the confidence of generalizing the solution. The following conclusions can be drawn from this study.

- For the pre-decided topology and nodal coordinates (geometry) of a tensegrity, it is possible to find an optimum self-stress state such that the structure has relatively high stiffness with its low natural frequencies being separated.
- Two approaches were used to construct the self-stress vector, scaling from the self-stress of one module or a linear combination of the independent self-stress vectors of all modules. Then, GA was used to find the optimum self-stress vector. It has been shown, that the optimum self-stress vectors obtained by both approaches are approximately equal for the maximization and separation of the lower natural frequencies.
- It is important to introduce also functional constraints for the real work of the structure, not only VHM criteria.
- The Genetic Algorithm can give practically relevant results for the stated problem, even if final convergence and global optimality are difficult to prove. The weight factors used to bring the multi-objective criteria into one fitness function can be tuned to specific needs, relying on the assumed continuity of the optima.

For future work, we suggest the following two points:

- When regulating the pre-stress level in each module to satisfy the above requirements, the ratio between the internal forces and the diameter of each component must be considered. This will reduce the amount of material used and hence the weight of the structure. It is interesting to study the proposed optimization problem with the aspects of tensegrity structures mass reduction (Nagase and Skelton, 2014a, 2014b; Skelton and de Oliveira, 2009).
- In this study the focus was only on the separation of first two sensitive natural frequencies. In the nearest future we will try to separate at least the first 6 modes using different objective function but with the same constraints. It is fully conceivable to introduce several septation criteria in the combined cost function.

Appendix A

To find the self-stress vector of the whole structure $\boldsymbol{g}_\psi$ by scaling the self-stress vector $\boldsymbol{s}_0$ of the base module, we first calculate the self-stress vector $\boldsymbol{s}_0$ of the base module from the SVD of its equilibrium matrix $\boldsymbol{A}$, constructed from the topology, coordinates and numbering scheme given in Fig. 1(a). The equilibrium matrix $\boldsymbol{A}$ was constructed following the method in Tran and Lee (2010b), Schek (1974). The SVD of $\boldsymbol{A}$ gives the unique self-stress vector $\boldsymbol{s}_0$ of the base module.

$\boldsymbol{s}_0 = \begin{bmatrix} 0.44721 & 0.22360 & 0.44721 & 0.22360 & -0.50 & -0.50 \end{bmatrix}^T$

and after normalization by $|s_i|$ value of one of the bars, (here, s_6) the final vector $\boldsymbol{s}_0$ becomes:

$\boldsymbol{s}_0 = \begin{bmatrix} 0.89442 & 0.44721 & 0.89442 & 0.44721 & -1 & -1 \end{bmatrix}^T$

Then, from Eq. (1) the self-stress vector of each module was found as:

$\boldsymbol{s}_1 = a_1\boldsymbol{s}_0$, $\boldsymbol{s}_2 = a_2\boldsymbol{s}_0$, $\boldsymbol{s}_3 = a_3\boldsymbol{s}_0$, and $\boldsymbol{s}_4 = a_4\boldsymbol{s}_0$, with a size of each vector of 6×1.

All modules have the same numbering scheme as the base module in Fig. 1(a).

The structure self-stress vector $\boldsymbol{g}_\psi$ is constructed with shared components between modules being added to gather and following the numbering scheme of the whole structure in Fig. 1(b):

$$\boldsymbol{g}_\psi = \begin{bmatrix} s_1^1,\ s_2^1,\ s_3^1,\ s_4^1,\ s_4^2,\ s_4^3,\ s_3^3,\ s_2^3,\ s_1^3,\ s_1^4,\ (s_1^2+s_2^4),\ (s_2^2+s_3^4), \\ \times\ (s_3^2+s_4^4),\ s_1^5,\ s_1^6,\ s_2^5,\ s_2^6,\ s_3^5,\ s_3^6,\ s_4^5,\ s_4^6 \end{bmatrix}$$

where s_i^m means the element m in $\boldsymbol{s}_i$ of the module i.

Appendix B

The mathematical expression of the 3-D element elastic $\boldsymbol{k}_E$, geometric $\boldsymbol{k}_G$ and mass $\boldsymbol{m}$ matrices:

$$\boldsymbol{k}_E = \begin{bmatrix}
\frac{EA}{l} & 0 & 0 & 0 & 0 & 0 & \frac{-EA}{l} & 0 & 0 & 0 & 0 & 0 \\
0 & \frac{12EI_z}{l^3} & 0 & 0 & 0 & \frac{6EI_z}{l^2} & 0 & \frac{-12EI_z}{l^3} & 0 & 0 & 0 & \frac{6EI_z}{l^2} \\
0 & 0 & \frac{12EI_y}{l^3} & 0 & \frac{-6EI_y}{l^2} & 0 & 0 & 0 & \frac{-12EI_y}{l^3} & 0 & \frac{-6EI_y}{l^2} & 0 \\
0 & 0 & 0 & \frac{GI_x}{l} & 0 & 0 & 0 & 0 & 0 & \frac{-GI_x}{l} & 0 & 0 \\
0 & 0 & \frac{-6EI_y}{l^2} & 0 & \frac{4EI_y}{l} & 0 & 0 & 0 & \frac{6EI_y}{l^2} & 0 & \frac{2EI_y}{l} & 0 \\
0 & \frac{6EI_z}{l^2} & 0 & 0 & 0 & \frac{2EI_z}{l} & 0 & \frac{-6EI_z}{l^2} & 0 & 0 & 0 & \frac{2EI_z}{l} \\
\frac{-EA}{l} & 0 & 0 & 0 & 0 & 0 & \frac{EA}{l} & 0 & 0 & 0 & 0 & 0 \\
0 & \frac{-12EI_z}{l^3} & 0 & 0 & 0 & \frac{-6EI_z}{l^2} & 0 & \frac{12EI_z}{l^3} & 0 & 0 & 0 & \frac{-6EI_z}{l^2} \\
0 & 0 & \frac{-12EI_y}{l^3} & 0 & \frac{6EI_y}{l^2} & 0 & 0 & 0 & \frac{12EI_y}{l^3} & 0 & \frac{6EI_y}{l^2} & 0 \\
0 & 0 & 0 & \frac{-GI_x}{l} & 0 & 0 & 0 & 0 & 0 & \frac{GI_x}{l} & 0 & 0 \\
0 & 0 & \frac{-6EI_y}{l^2} & 0 & \frac{2EI_y}{l} & 0 & 0 & 0 & \frac{6EI_y}{l^2} & 0 & \frac{4EI_y}{l} & 0 \\
0 & \frac{6EI_z}{l^2} & 0 & 0 & 0 & \frac{2EI_z}{l} & 0 & \frac{-6EI_z}{l^2} & 0 & 0 & 0 & \frac{4EI_z}{l}
\end{bmatrix}$$

$$\boldsymbol{k}_G = \frac{T}{l} \begin{bmatrix}
0 & 0 & 0 & 0 & 0 & 0 & 0 & 0 & 0 & 0 & 0 & 0 \\
0 & \frac{6}{5} & 0 & 0 & 0 & \frac{l}{10} & 0 & \frac{-6}{5} & 0 & 0 & 0 & \frac{l}{10} \\
0 & 0 & \frac{6}{5} & 0 & \frac{-l}{10} & 0 & 0 & 0 & \frac{-6}{5} & 0 & \frac{l}{10} & 0 \\
0 & 0 & 0 & \frac{j_x}{A_x} & 0 & 0 & 0 & 0 & 0 & \frac{-j_x}{A_x} & 0 & 0 \\
0 & 0 & \frac{-l}{10} & 0 & \frac{2l^2}{15} & 0 & 0 & 0 & \frac{l}{10} & 0 & \frac{-l^2}{30} & 0 \\
0 & \frac{l}{10} & 0 & 0 & 0 & \frac{2l^2}{15} & 0 & \frac{-l}{10} & 0 & 0 & 0 & \frac{-l^2}{30} \\
0 & 0 & 0 & 0 & 0 & 0 & 0 & 0 & 0 & 0 & 0 & 0 \\
0 & \frac{-6}{5} & 0 & 0 & 0 & \frac{-l}{10} & 0 & \frac{6}{5} & 0 & 0 & 0 & \frac{-l}{10} \\
0 & 0 & \frac{-6}{5} & 0 & \frac{l}{10} & 0 & 0 & 0 & \frac{6}{5} & 0 & \frac{l}{10} & 0 \\
0 & 0 & 0 & \frac{-j_x}{A_x} & 0 & 0 & 0 & 0 & 0 & \frac{j_x}{A_x} & 0 & 0 \\
0 & 0 & \frac{l}{10} & 0 & \frac{-l^2}{30} & 0 & 0 & 0 & \frac{l}{10} & 0 & \frac{2l^2}{15} & 0 \\
0 & \frac{l}{10} & 0 & 0 & 0 & \frac{-l^2}{30} & 0 & \frac{-l}{10} & 0 & 0 & 0 & \frac{2l^2}{15}
\end{bmatrix}$$

$$\boldsymbol{m} = \rho A l \begin{bmatrix}
\frac{1}{3} & 0 & 0 & 0 & 0 & 0 & \frac{1}{6} & 0 & 0 & 0 & 0 & 0 \\
0 & \frac{13}{35} & 0 & 0 & 0 & \frac{11l}{210} & 0 & \frac{9}{70} & 0 & 0 & 0 & \frac{-13l}{420} \\
0 & 0 & \frac{13}{35} & 0 & \frac{-11l}{210} & 0 & 0 & 0 & \frac{9}{70} & 0 & \frac{13l}{420} & 0 \\
0 & 0 & 0 & \frac{I_x}{3A} & 0 & 0 & 0 & 0 & 0 & \frac{I_x}{6A} & 0 & 0 \\
0 & 0 & \frac{-11l}{210} & 0 & \frac{l^2}{105} & 0 & 0 & 0 & \frac{-13l}{420} & 0 & \frac{-l^2}{140} & 0 \\
0 & \frac{11l}{210} & 0 & 0 & 0 & \frac{l^2}{105} & 0 & \frac{13l}{420} & 0 & 0 & 0 & \frac{-l^2}{140} \\
\frac{1}{6} & 0 & 0 & 0 & 0 & 0 & \frac{1}{3} & 0 & 0 & 0 & 0 & 0 \\
0 & \frac{9}{70} & 0 & 0 & 0 & \frac{13l}{420} & 0 & \frac{13}{35} & 0 & 0 & 0 & \frac{-11l}{210} \\
0 & 0 & \frac{9}{70} & 0 & \frac{-13l}{420} & 0 & 0 & 0 & \frac{13}{35} & 0 & \frac{11l}{210} & 0 \\
0 & 0 & 0 & \frac{I_x}{6A} & 0 & 0 & 0 & 0 & 0 & \frac{I_x}{3A} & 0 & 0 \\
0 & 0 & \frac{13l}{420} & 0 & \frac{-l^2}{140} & 0 & 0 & 0 & \frac{11l}{210} & 0 & \frac{l^2}{105} & 0 \\
0 & \frac{-13l}{420} & 0 & 0 & 0 & \frac{-l^2}{140} & 0 & \frac{-11l}{210} & 0 & 0 & 0 & \frac{l^2}{105}
\end{bmatrix}$$

References

Ali, N.B.H., Rhode-Barbarigos, L., Albi, A.A.P., Smith, I.F., 2010. Design optimization and dynamic analysis of a tensegrity-based footbridge. Eng. Struct. 32 (11), 3650–3659.

Argyris, J., Mlejnek, H.-P., 1991, vol. V. Dynamics of Structures. Text on Computational Mechanics. Elsevier Science Publishers, Amsterdam.

Ashwear, N., Eriksson, A., 2014. Natural frequencies describe the pre-stress in tensegrity structures.. Comput. Struct. 138, 162–171.

Ashwear, N., Eriksson, A., 2015. Influence of temperature on the vibration properties of tensegrity structures. Int. J. Mech. Sci. 99, 237–250.

Barbosa, H., Bernardino, H., Angelo, J., 2015. In: Tosmpanakis, Y., Kruis, J., Topping, B. (Eds.), Derivative-free techniques for multiobjective structural optimization: a review, 12. Sax-CoburgPublications, Stirlingshire, Scotland, pp. 27–52.

Buchholdt, H., 1969. A non-linear deformation theory applied to two dimensional pretensioned cable assemblies. In: Proc. Inst. Civ. Eng., 42, pp. 129–141.Thomas Telford.

Caramia, M., Dell'Olmo, P., 2008. Multi-objective Management in Freight Logistics: Increasing Capacity, Service Level and Safety with Optimization Algorithms. Springer, London.

Dalilsafaei, S., Eriksson, A., Tibert, G., 2014. Optimum pre-stress design for frequency requirement of tensegrity structures. Blucher Mech. Eng. Proc. 1 (1), 1258–1270.

Dalilsafaei, S., Tibert, G., 2012. Design and analysis of tensegrity power lines. Int. J. Space Struct. 27 (2–3), 139–154.

Eriksson, A., 1997. Equilibrium subsets for multi-parametric structural. Comput. Methods Appl. Mech. Eng. 140 (3–4), 305–327.

Faroughi, S., Tur, J., 2015. Vibration properties in the design of tensegrity structure. J. Vib. Control 21 (3), 611–624.
Guechaichia, A., Trendafilova, I., 2011. A simple method for enhanced vibration-based structural health monitoring. J. Phys. Conf. Ser. 305 (1), 012073.
Holland, J.H., 1975. Adaptation in Natural and Artificial Systems. University of Michigan Press, Ann Arbor, MI, USA.
Kattan, P., 2007. MATLAB Guide to Finite Elements: An Interactive Approach. Springer, Berlin.
Kebiche, K., Kazi-Aoual, M., Motro, R., 1999. Geometrical non-linear analysis of tensegrity systems. Eng. Struct. 21 (9), 864–876.
Koohestani, K., 2012. Form-finding of tensegrity structures via genetic algorithm. Int. J. Solids Struct. 49 (5), 739–747.
Koohestani, K., 2013. A computational framework for the form-finding and design of tensegrity structures. Mech. Res. Commun. 54, 41–49.
Koohestani, K., 2015. Automated element grouping and self-stress identification of tensegrities. Eng. Comput. 32 (6), 1643–1660.
Koohestani, K., Guest, S., 2013. A new approach to the analytical and numerical form-finding of tensegrity structures. Int. J. Solids Struct. 50 (19), 2995–3007.
Kwan, A.S.K., 1996. Geometric non-linearity in cable networks. ASME, Petroleum Division (Publication) PD 73 (1), 93–97.
Lewis, W., Jones, M., Rushton, K., 1984. Dynamic relaxation analysis of the non-linear static response of pretensioned cable roofs. Comput. Struct. 18 (6), 989–997.
Masic, M., Skelton, R.E., 2006. Selection of prestress for optimal dynamic/control performance of tensegrity structures. Int. J. Solids Struct. 43 (7–8), 2110–2125.
Motro, R., 2003. Tensegrity: Structural Systems for the Future, first ed. Kogan Page Science, London.
Moussa, B., Ben Kahla, N., Pons, J.C., 2001. Evolution of natural frequencies in tensegrity systems: a case study. Int. J. Space Struct. 16 (1), 57–73.
Murakami, H., Nishimura, Y., 2001. Initial shape finding and modal analyses of cyclic right-cylindrical tensegrity modules. Comput. Struct. 79 (9), 891–917.
Nagase, K., Skelton, R., 2014a. Minimal mass design of tensegrity structures. Proc. SPIE Int. Soc. Opt. Eng. 9061 90610W-90610W-14.
Nagase, K., Skelton, R., 2014b. Minimal mass tensegrity structures. J. Int. Assoc. Shell Spatial Struct. 55 (1), 37–48.
Nishimura, Y., Murakami, H., 2001. Initial shape-finding and modal analyses of cyclic frustum tensegrity modules. Comput. Methods Appl. Mech. Eng. 190 (43–44), 5795–5818.
Paultre, P., 2010. Dynamics of Structures. ISTE Wiley, London.
Peeters, B., De Roeck, G., 2001. One-year monitoring of the Z24-bridge: environmental effects versus damage events. Earthquake Eng. Struct. Dyn. 30 (2), 149–171.
Pinaud, J., Solari, S., Skelton, R.E., 2004. Deployment of a class 2 tensegrity boom. Proc. SPIE Int. Soc. Opt. Eng. 5390, 155–162.
Schek, H.-J., 1974. The force density method for form finding and computation of general networks. Comput. Methods Appl. Mech. Eng. 3 (1), 115–134.
Schlaich, M., 2004. The messeturm in rostock – a tensegrity tower. J. Int. Assoc. Shell Spatial Struct. 45 (145), 93–98.
Skelton, R.E., de Oliveira, M.C., 2009. Tensegrity Systems. Springer, London.
Strang, G., 1988. Linear Algebra and Its Applications, third ed. Thomson Learning, USA.
Sultan, C., 2009. Designing structures for dynamical properties via natural frequencies separation. application to tensegrity structures design. Mech. Syst. Sig. Process 23 (4), 1112–1122.
Tibert, A.G., Pellegrino, S., 2002. Deployable tensegrity reflectors for small satellites. J. Spacecr. Rockets 39 (5), 701–709.
Tran, H.C., Lee, J., 2010a. Advanced form-finding for cable-strut structures. Int. J. Solids Struct. 47 (14–15), 1785–1794.
Tran, H.C., Lee, J., 2010b. Initial self-stress design of tensegrity grid structures. Comput. Struct. 88 (9–10), 558–566.
Tran, H.C., Lee, J., 2010c. Self-stress design of tensegrity grid structures with exostresses. Int. J. Solids Struct. 47 (20), 2660–2671.
Tran, H.C., Lee, J., 2011. Geometric and material nonlinear analysis of tensegrity structures. Acta Mech. Sin. 27 (6), 938–949.
Vassart, N., Motro, R., 1999. Multiparametered form finding method: Application to tensegrity systems. Int. J. Space Struct. 14 (2), 147–154.